Atmospheric
Chemistry
and Physics
Discussions

New Particle Formation at a High Altitude Site in India: Impact of Fresh Emissions and Long Range Transport

Vyoma Singla, Subrata Mukherjee*, Adam Kristensson, Govindan Pandithurai, Kundan K. Dani, Vasudevan Anil Kumar

Indian Institute of Tropical Meteorology, Pune

*Corresponding author: subrata.cat@tropmet.res.in

Abstract

There is a lack of characterization of the aerosol population in Western India, how it is affected by meteorological parameters, and new particle formation and the influence on cloud condensation nuclei (CCN). For this reason, measurements of particle number size distribution, aerosol chemical composition, meteorology and cloud condensation nuclei number concentration were monitored at High Altitude Cloud Physics Laboratory (HACPL) in Mahabaleshwar mountain town in Western India between November 2016 and February 2017. Most air masses in this period originated from the Indian continent to the north-east of HACPL. New particle formation (NPF) events were observed on 47 days and mainly associated with these north-easterly air masses and high SO_2 emissions and biomass burning activities, while weaker or non-NPF days were associated with westerly air masses and relatively higher influence of local air pollution. The growth of newly formed particles enhanced the mass concentration of secondary organic and inorganic species of aerosol particles. The mean growth rate, formation rate, condensation sink and coagulation loss for the 13 strongest events was found to be 2.6 ± 0.4 nm h^{-1}, 2.8 ± 1.4 cm^{-3} s^{-1}, 2.2 ± 2.9 *10^{-2} s^{-1} and 1.6 ± 1.0 cm^{-3} s^{-1} respectively. A closer examination of strong NPF events showed that low relative humidity and solar radiation favoured new particle formation. These NPF events lead to a significant increase in CCN concentration (mean ~53 ± 36 %). The NanoMap method revealed that NPF took place up to several hundred kilometers upwind and to the north-east of HACPL.

1. Introduction

Atmospheric aerosols directly affect the global climate by altering the radiative balance of the Earth atmosphere system (Stier et al., 2007) and indirectly by altering the cloud properties (Fan et al., 2012). However, these effects depend on the particle number size distribution and chemical composition of aerosol particles. Recent studies have shown that particle size is more important than the chemical composition in cloud formation (Dusek et al., 2006; Rose et al., 2010). The particles in the upper Aitken mode (>50 nm diameter) and in the accumulation mode (100-1000 nm) have a substantial effect on the cloud properties and initiation of precipitation as cloud condensation nuclei (Rosenfeld et al., 2008). Further, the number concentration of accumulation mode particles is related to visibility degradation (See et al., 2006), and sub-micron particles with health related problems (Seaton and Denekamp, 2003).

New particle formation (NPF) is one of the major sources of sub-micron particles in the atmosphere. It is characterized by a significant enhancement in the number concentration of nucleation mode particles and subsequent growth of these nucleated particles due to condensation (Kulmala and Kerminen, 2008; Skrabalova et al., 2015). Typical formation rates (FR) of 3 nm particles are in the range 0.01-10 cm^{-3} s^{-1} and typical growth

41 rates (GR) in the range 1-20 nm h^{-1}, depending upon temperature, humidity, pressure, and availability of

42 condensable vapours. In urban areas, FR is often higher ~100 cm^{-3} s^{-1} and even higher in the coastal areas and

43 industrial plumes ~ 10^7-10^5 cm^{-3} s^{-1} (Kulmala et al., 2004). The atmospheric observations and laboratory

44 experiments have identified sulfuric acid and organics as the two important precursors of NPF (Riipinen et al.,

45 2007; Barsanti et al., 2009). There is always a competition between the FR and GR of freshly nucleated particles

46 and the condensation sink and coagulation sink with larger particles (Vehkamki and Riipinen, 2012). As a result

47 of that, nucleation and Aitken mode particles smaller than 25 nm and between 25 and 100 nm diameter,

48 respectively tend to have a shorter lifetime than accumulation mode particles between 0.1 and 1 µm diameter. If

49 the FR is large enough and the condensation and coagulation sinks low enough during NPF, these recently

50 generated particles can survive long enough in the atmosphere to be transported over distances of several

51 hundred kilometers, depending on the wind speed (Kivekas et al., 2016).

52

53 The measurements of particle number size distribution show that NPF events and growth are widespread

54 (Kulmala et al., 2004; Kulmala and Kerminen, 2008; Gong et al., 2008; Yue et al., 2010). Many studies address

55 the spatial scale of NPF events in which the horizontal scale of NPF extends from hundreds to thousands of

56 kilometres (Kulmala et al., 2004; Stainer et al., 2004; Dal Maso et al., 2005; Yue et al., 2010, Kristenson et al.,

57 2014). The spatial scale of NPF events help to identify the origin of nucleation mode particles (Nemeth and

58 Salma, 2014; Väänänen et al., 2016; Shen et al., 2018). The newly formed particles become climatically

59 important when they attain the size of ~50 nm in diameter (Kerminen et al., 2012). The particles with diameter ≥

60 50 nm tend to act as CCN and affect the cloud microphysical and optical properties (Fiore et al., 2012). Model

61 studies show that NPF accounts for 5-50% of the CCN number concentration in the boundary layer (Spracklen

62 et al., 2008). A study by Wiedensohler et al.(2009) shows that the growing nucleation mode particles can

63 contribute to about 80% of the CCN number concentration during special conditions with strong NPF in China.

64 Several other studies report the significant enhancement in atmospheric CCN concentrations due to NPF events

65 (Levin et al., 2012; Creamean et al., 2011; Yue et al., 2011; Pierce et al., 2012; Ma et al., 2016; de Espana et al.,

66 2017). NPF is known to dominate the particle number concentrations in clean atmosphere as compared to

67 anthropogenically influenced regions (Lihavainen, 2003). However, the detailed mechanism of nucleation, its

68 growth and its connection with biogenic emissions, anthropogenic activities and atmospheric chemistry, and the

69 global role for CCN is still uncertain.

70

71 In this study, we identify the NPF events by analyzing particle number size distribution (PNSD) data at HACPL,

72 Mahabaleshwar between November 2016 and February 2017. The characteristics of PNSD, new particle

73 formation rate (FR), growth rate (GR) and condensation sink (CS) are evaluated during the identified NPF

74 events at HACPL. The role of meteorology and chemical composition of sub-micron non-refractory particulate

75 matter (NR-PM$_1$) during the growth of freshly nucleated particles is also analyzed. A cluster analysis is

76 performed to identify the geographical source areas responsible for the observed NPF events. The spatial scale

77 of NPF events and where the 1-2 nm diameter particles are formed around the station is also analyzed by using

78 the NanoMap method (Kristensson et al., 2014). Finally, the measured CCN number concentration, PNSD

79 (5.14-900 nm) and chemical composition of NR-PM$_1$ aerosol are used to evaluate the probable contribution of

80 NPF to the total CCN concentration at the sampling site.

Atmospheric
Chemistry
and Physics
Discussions

81

2. Methodology

2.1 Measurement Site

84 Measurements were performed at HACPL (17.92° N, 73.65° E; 1378 m above mean sea level), located in the

85 Western Ghats mountain range in south-west India. The site is at the small hill town Mahabaleshwar, which is

86 also a tourist attraction. The town is surrounded by dense vegetation and residential houses, hotels and a rural

87 market. During the study period, the site was influenced by both, local and regional anthropogenic pollution

88 depending on the meteorological conditions and timing of source activities (Mukherjee et al., 2018).

89

2.2 Instrumentation

91 The aerosol chemical composition, particle number concentration and cloud condensation nuclei (CCN) number

92 concentration were measured by using Time of Flight - Aerosol Chemical Speciation Monitor (ToF-ACSM),

93 Wide Range Aerosol Spectrometer (WRAS) and CCN counter (CCNC) respectively. Due to different temporal

94 resolutions of these instruments, the data sets were averaged hourly for the analysis. The QA/QC procedure for

95 ToF-ACSM can be found in Mukherjee et al. (2018) and for WRAS and CCNC in Singla et al. (2017). The

96 meteorological conditions (Solar radiation (SR), surface temperature (T), relative humidity (RH), wind speed

97 (WS) and wind direction (WD)) were recorded using an Automatic Weather Station (AWS) at an interval of one

98 minute.

99

2.2.1 Time of Flight - Aerosol Chemical Speciation Monitor (ToF-ACSM)

101 A detailed description, specific to our ACSM instrument, its operation and calibration procedure is discussed in

102 our earlier work (Mukherjee et al., 2018). In brief, before the ACSM, we sample the particle-laden and particle

103 free air alternatively and then focus the particle beam into ACSM through an aerodynamic lens. In the detection

104 chamber, the non-refractory particle fraction vaporizes at ~600∘C and ~10^{-7} mbar and is subsequently ionized

105 by the electron impaction ($E_{kin} = 70$ eV) by a tungsten filament arranged perpendicular to the particle beam in

106 the vaporization region. The ions are extracted by a set of ion optics and introduced into the TOF analyzer

107 where they are orthogonally extracted and separated based on their mass-to-charge ratio. The lens system has

108 almost 100 % transmission at vacuum aerodynamic diameters between 150–450 nm (Liu et al., 2007). The

109 collection efficiency is assumed to be 0.5 in this analysis.

110

2.2.2 Wide-range aerosol spectrometer (WRAS)

112 The aerosol particle number concentration (PNC) was measured as a function of particle size (range ~ 5 nm to

113 32 μm in 72 channels) at 4-minute interval by using WRAS (manufactured by Grimm, Germany). The detailed

114 description and calibration procedure of WRAS can be found in Singla et al., 2017. The instrument is kept under

115 air conditioning conditions for its running at constant temperature. The sampling probe features a Nafion dryer

116 to reduce the humidity to ~40%, to avoid the effect of ambient humidity and to reduce the error in measuring

117 diameter in the detection system. Although WRAS provides information in the size range of 5 nm - 32 μm, we

118 have used PNC in the size range of 5.14 – 900 nm only to identify the NPF events in this study.

119

2.2.3 Cloud Condensation Nuclei Counter (CCNC)

121 Our earlier work (Singla et al., 2017) gives the detailed description of the CCN counter used in this study. A

122 similar procedure was followed for the calibration of CCNC as discussed in Singla et al., 2017. The CCN

123 number concentration was monitored as a function of time and supersaturation (SS) using a single-column

124 continuous flow stream wise thermal gradient CCN chamber (DMT CCNC-100; Lance et al., 2006; Roberts and

125 Nenes, 2005). The instrument runs at a flow rate of 0.5 Lmin^{-1} with a sheath-to-aerosol flow ratio of 10:1. The

126 activated particles are subsequently sized using an optical particle counter (OPC) and counted as CCN in the

127 diameter range of 0.75 – 10 µm. The instrument samples particles every second at five different SS (0.1, 0.3,

128 0.5, 0.7 and 0.9%). The CCN concentration at 0.1% SS is measured for 10 min and 5 min each for every other

129 SS. This gives one complete CCN SS spectra in half an hour. The CCN data was only used in the period when

130 the temperature was stable at each SS level.

131

132 **3. Data Analysis**

133 **3.1 Parameters characteristic of NPF events**

134 The criteria prescribed by Dal Maso et al.(2005) have been used for classifying the NPF events. The parameters

135 characteristic of NPF events - growth rate (GR), formation rate (FR), condensation sink (CS) and coagulation

136 loss (Coag) were calculated following the methodology of Dal Maso et al.(2005). The FR of 5nm particles was

137 calculated at the beginning of each event and is expressed as:

138

139 $$J_5 = \frac{dN_{5-25}}{dt} + F_{coag} + F_{growth}$$

140

141 where N_{5-25} is the concentration of nucleation mode particles (N_{nuc}), F_{coag} is the scavenging of particles due to

142 coagulation of freshly nucleated particles and F_{growth} is the flux of particles growing out of the size range 5-25

143 nm. This growing flux of particles is defined as:

144

145 $$F_{growth} = \frac{1}{\Delta Dp}.GR_{5-25}.N_{5-25}$$

146

147 where ΔDp is the change in diameter of particle i.e. 25nm - 5nm = 20 nm, in this case. GR_{5-25} is the growth rate

148 of freshly nucleated particles in the size range ~5-25 nm. The GR was obtained by fitting a first-order

149 polynomial to the geometric mean diameters (GMD) of the nucleation mode particles. It is defined as:

150

151 $$GR_{5-25} = \frac{\Delta Dp}{\Delta t}$$

152

153 Here ΔD_p is the change in geometric mean diameter and Δt is the time interval. Further, the coagulation loss

154 term, F_{coag} is defined as:

155

156 $$F_{coag} = N_{5-25}.\,Coag_{5-25}$$

157 and $$Coag_{5-25} = \sum_j K_{ij}N_j$$

158

Atmospheric
Chemistry
and Physics
Discussions

159 Coag$_{5-25}$ is the coagulation loss rate. K$_{ij}$ is the coagulation coefficient between size bin 'i' and 'j' and N$_j$ is the

160 PNC in size bin 'j'. Here 'i' was represented by 8 nm diameter and 'j' was varied between 25 and 900 nm

161 diameter. Following Seinfeld and Pandis, 2008, the coagulation coefficient was calculated as:

162

163
$$K_{ij} = \frac{2kT}{3\mu} \frac{(D_{pi} + D_{pj})^2}{(D_{pi} \times D_{pj})}$$

164

165 Here 'Dp' is the particle diameter, k is the Boltzmann constant (1.38 x 10^{-19} cm^2 kg s^{-1}), μ is the viscosity of air

166 (1.81 x 10^{-7} kg cm^{-1}) and T is the surface temperature in Kelvin. Next, the condensation sink was calculated

167 based on the assumption that the properties of condensable vapors were similar to sulfuric acid, an important

168 condensable gas for the condensational growth of nucleated particles (Kulmala et al., 2013). CS is defined as:

169

170
$$CS = 2\pi \, . \, D_j \, . \sum_j \beta_{mj} \, . \, d_j . \, N_j$$

171 where D is the diffusion coefficient for sulfuric acid ~0.117 cm^{-2}s^{-1} (Gong et al., 2010) and β_{mj} is the size

172 dependent transition correction factor. The number concentration of aerosol particles in the size range of 5-25

173 nm was used to estimate the FR and GR. The CS and F$_{coag}$ were calculated using the entire PSND (~5-900 nm).

174 The units of FR, GR, CS and F$_{coag}$ are cm^{-3}s^{-1}, nm h^{-1}, s^{-1} and cm^{-3}s^{-1} respectively.

175

176 **3.2 NanoMap**

177 The NanoMap method developed by Kristensson et al.(2014), aims at representing the spatial distribution of

178 regional NPF events based on the meteorological backward trajectories and continuous PNSD measurements at

179 a point station. NanoMap gives an estimation of where NPF takes place at the point of formation of 1.5 nm

180 diameter particles up to at least 500 km distance upwind of the sampling site. This method is based on the

181 assumption that the measured NPF is a regional event and takes place over the full area covered by the regional

182 NPF event with the same nucleation start and end time. The NanoMap procedure follows four basic steps - (i)

183 classification and identification of type I NPF events (ii) choosing the start and end time of particle formation at

184 the lowest bin size (iii) determining the end of growth time i.e. the growth of newly formed particles can no

185 longer be followed in size distribution spectrum and (iv) plotting of a geographical position of the NPF events

186 based on the meteorological backward trajectories and selection made in steps i) to iii). The meteorological

187 backward trajectories have been calculated using the HYSPLIT model and meteorology data input from 1°

188 resolution Global Data Assimilation System (GDAS, Draxler and Rolph, 2003).

189

190 NanoMap is intended both for short data set (months to a few years) and longer data sets (several years or

191 longer, where even the probability of formation as a function of geographical region can be estimated). In this

192 study, the dataset of four months (from November 2016 to February 2017) is used to explore where the events

193 take place. The lowest detection limit diameter of WRAS is 5 nm and nucleated particles need some time to

194 grow from the initial size of 1.5 nm (Kulmala et al., 2013). The time shift between the real time formation and

195 observed time formation of particles was set to 1.5h based on the reported mean GR (~2.58 nm h^{-1}) at the

196 sampling site. Uncertainties related to event classification, selection of starting and ending times, simultaneous

197   event assumption and trajectory uncertainty are not negligible for the NanoMap method (Kristensson et al.,
198   2014).

199

200   **4. Results and Discussion**

201   The PNSD data measured during the study period were analyzed to identify the NPF events at HACPL. NPF

202   events occurred on ~40% of the measurement days (47 days out of 115 days). Of the total 47 NPF events, 13

203   events were identified as strong events and 34 events as weak events. The strong and weak events were

204   classified based on the number concentration of nucleation mode particles during the event. The events with

205   N_{nuc} concentration greater than $6.0*10^3$ cm^{-3} were referred to as strong NPF events and vice-versa. Out of these

206   47 NPF events, a strong event day (12th December 2016) was selected for a more detailed analysis. The

207   sampling site was under a varying influence of regional pollution throughout the study period (Mukherjee et al.,

208   2018). The characteristics of NPF were studied in terms of growth rate (GR), condensation sink (CS), formation

209   rate (FR) and coagulation (F_{coag}). The characteristics of the NPF day were compared with the non-NPF day -

210   14th December 2016. The role of meteorology and aerosol chemical composition on NPF was also evaluated.

211   Further, the contribution of newly formed particles to CCN was evaluated.

212

213   **4.1 Characteristics of NPF and non-NPF Event**

214   Figure 1 gives the colorplot of size distribution of aerosol particles on 12th and 14th December. In general, the

215   formation of new particles is governed by (i) precursor gases (ii) meteorological conditions like solar radiation,

216   temperature, relative humidity and wind speed and (iii) condensation sink. Figure 2 gives the diurnal variation

217   of different meteorological parameters on the NPF and non-NPF day. During the NPF day, there was a sharp

218   decrease in PNC from $~5.8*10^3$ cm^{-3} to $4.1*10^3$ cm^{-3} at 08:00 hrs. This decrease was related to an increase in the

219   boundary layer height. The gradual increase in boundary layer height is believed to bring cleaner air from aloft

220   to the ground, thereby lowering the CS to about $1.8*10^{-2}$ s^{-1} a few hours later. Under low CS conditions, a

221   sudden enhancement in the concentration of N_{nuc} ($~1.3*10^4$ cm^{-3}) was observed at 11:00 hrs. The formation rate

222   (J_5) of particles was calculated as $~6.6$ cm^{-3} s^{-1}. The CS is a measure of the amount of surface of the pre-existing

223   aerosol particles available for the semi-volatile gases to condense on to. Thus the low aerosol surface favoured

224   accumulation of condensable species in the gas phase, which nucleated and grew the new particles. The

225   formation of new particles was observed approximately 60-90 minutes later than the onset of photo-oxidation.

226   This delay was likely due to the lower limit of WRAS (5.14 nm) where it takes some time for nucleated cluster

227   particles at 1.5 nm diameter to grow to the detectable size at 5.14 nm). This is also the reason why the

228   representative value of CS in Table 1 at the onset of nucleation is chosen as one hour prior to the first observed

229   nucleation by the WRAS at 5.14 nm. During the nucleation process, high solar radiation (mean $~437\pm31$ Wm^{-2}),

230   low relative humidity (mean $~28\pm3$ %) and low wind speed (mean $~3\pm0.7$ ms^{-1}) were recorded. This hot and

231   less humid condition tends to favour the enhancement of atmospheric nucleation (Hamed et al., 2011).

232   According to Figure 1, the particles were continuously formed at 5 nm diameter for a minimum of 2 hours and

233   then grew at a rate of 2.5 nm hr^{-1} (12th Dec) to a median size of 40 nm in due course of approximately 6 hours.

234   The growth of particles shifted in the particle size distribution from nucleation to an Aitken (N_{ait}) and/or

235   accumulation (N_{acc}) regime in the early morning of 13th December (01:00 hrs). Similar type of nucleation events

236   have been observed by other researchers (Dal Maso et al., 2005; Kulmala et al., 2004; Wu et al., 2007; Wang et

237   al., 2013; Kanawade et al., 2014; Leena et al., 2016; de Espana et al., 2017; Li et al., 2017). The CS increased

238   gradually during the event with its hourly averaged maximum ($4.9*10^{-2}$ s^{-1}) around 18:00 hrs, demonstrating

239   that the photo-oxidation has caused the rapid production of condensable vapors (Figure S1). The diurnal

240   variation of coagulation sink with its peak (hourly maximum ~ 9 cm^{-3} s^{-1}) at 13:00 hrs suggested the maximum

241   coagulation removal of newly formed particles during this time period (Figure S1). The coagulation sink for

242   other strong NPF days is reported as an average throughout the day ± standard deviation in Table 1.

243

244   On the other hand, the non-NPF day (14th December) tended to have particle size distribution without a peak in

245   N_{nuc} and contained only N_{ait} and/or N_{acc} particles. The mean PNC during 11:00-16:00 hours was observed to be

246     $6.6*10^3 \pm 1.5*10^3$ cm^{-3} with the GMD calculated for the entire size distribution, varying between 45 to 80 nm.

247   During this period, high relative humidity (mean ~86 ± 4 %), high wind speed (mean ~6 ± 1 ms^{-1}) and low solar

248   radiation (mean ~238 ± 62 Wm^{-2}) was recorded. It is believed that high relative humidity (>80%) tends to limit

249   the availability of gaseous sulphuric acid (a key precursor for NPF formation) in ambient air and thus inhibits

250   the formation of new particles (Hamed et al., 2011).

251

252   The ambition was to calculate NPF parameters only during days with strong NPF. From the 13 strong NPF

253   event days, 3 of these had gaps in data for a few hours, and NPF parameters were not possible to calculate, and

254   hence only 10 strong events have been analyzed for NPF parameters. For these 10 events, the growth rate of

255   nucleation mode particles was found to be linear with an average growth rate of 2.6 ± 0.4 nm hr^{-1}. The CS on

256   NPF days was much lower than on non-NPF days (~4.2 - $4.4*10^{-2}$ s^{-1}). The characteristic parameters for all

257   strong NPF events days and 2 non-NPF days (for reference) are summarized in Table 1.

258

259   **4.2 Role of aerosol chemical composition**

260   Figure 3 gives the diurnal variation of N_{nuc} concentration, volume concentration of Aitken mode particles and

261   mass concentration of aerosol species for the strong NPF day during December 12, 2016. The role of these

262   parameters during the nucleation process was studied by dividing the activity period into 3-time windows. The

263   first window represents 09:30 to 11:00 hrs, which includes the formation of new particles. The window no. 2

264   from 11:00 to 13:30 hrs characterizes the increase in newly formed particles, and window no. 3 (13:30 to 18:00

265   hrs) represents the growth stage with an increase in volume concentration of Aitken mode particles and a

266   decrease in N_{nuc} concentration. During the first time window, a considerable decrease in aerosol mass

267   concentration coincided with the rising boundary layer height, which led to the dilution of pollutants. The N_{nuc}

268   concentration and Aitken volume concentration were at a minimum during this window. Since the formation of

269   new particles is governed by the nature of pre-existing aerosol particles, the particle acidity was evaluated by

270   following the methodology of Engelhardt et al., 2013. The ratio of ammonium to anions (sulfate and nitrate) was

271   calculated as 1.08, which indicated the neutralized nature of aerosols. The neutralized aerosols make the

272   atmospheric conditions favourable for NPF. On the other hand, the aerosols on non-NPF day (14th December)

273   were found to be slightly acidic in nature with the ratio of ammonium to anions varying between 0.88 and 0.90.

274   Therefore it is assumed that the ammonium available in atmosphere would be used up by the pre-existing anions

275   for their neutralization and thereby could potentially suppress the NPF (Pikridis et al., 2014). During window

276   no. 2, a significant increase in the N_{nuc} concentration was observed. In the third time window, the gradual

277   increase in Aitken volume concentration and decrease in N_{nuc} concentration was observed. This was
278   accompanied by the gradual increase in mass concentration of aerosol (organics, sulfate, nitrate and
279   ammonium), but with a time lag of ~2 hours. The ACSM is not able to detect the smallest particles in the Aitken
280   mode range, but only after they have grown to detectable sizes a few hours later. The organic components -
281   OOA, HOA, BBOA all increase during the afternoon and evening and were identified on the basis of
282   fragmentation patterns of the ACSM and source/receptor analysis of high resolution mass spectra using Positive
283   Matrix Factorization (PMF) model (Paatero and Tapper, 1994). More details on PMF methodology used in this
284   study are given in our earlier work (Mukherjee et al., 2018). OOA is the oxygenated organic aerosol and relates
285   to secondary organic aerosol. HOA and BBOA refer to hydrocarbon-like organic aerosol and biomass burning
286   organic aerosol. HOA and BBOA are the surrogates of primary organic aerosol. The gradual increase in aerosol
287   mass concentration suggested that (i) the particle size has grown large enough ($\geq$ 40 nm) to be able to be
288   detectable by the ACSM as explained earlier and (ii) that there is formation of secondary aerosol components
289   during the growth of newly formed particles. It is believed that the production of low volatile organic vapours
290   and nitrate have caused these new particles to grow quickly, thereby enhancing the CCN concentrations
291   significantly (Figure 3e). Similar features have also been reported by previous NPF studies in diverse
292   environments (Kulmala et al., 2004; Zhang et al., 2004; Crilley et al., 2014; Li et al., 2017).
293
294   **4.3 Contribution of NPF to CCN**
295   In order to become CCN, the freshly nucleated particles must attain a minimum size of ~40nm. To determine
296   the probable contribution of these particles to CCN, simultaneous measurements of CCN were carried out.
297   Figure 3(e) gives the hourly variation of CCN concentration at five supersaturation levels on the NPF day. The
298   CCN concentration increased gradually coinciding with the (i) increase in N_{ait} concentration, and (ii) increase in
299   volume concentration of Aitken mode particles. This increase in CCN concentration was attributed to the
300   increase in number concentration of particles fulfilling the size criteria for CCN formation. The probable
301   contribution of newly formed particles to CCN formation was evaluated in terms of percent increase in CCN.
302   The percent increase was calculated by comparing the CCN concentrations before and after the nucleation
303   event. The two time windows were selected as - "Window 1 (W_1) and Window 2 (W_2)" representing the time
304   periods before and after the nucleation event respectively (Please see Figure 1). While choosing these windows,
305   the care was taken to ensure that: (i) there were no primary emissions, (ii) meteorological conditions were
306   sufficiently stable, and (iii) the geometric mean diameter (GMD) of particles was well above 40 nm. In this
307   study, primary organic aerosol (POA= HOA+BBOA) was used as a marker for the primary emissions. The
308   stable meteorological conditions were defined by stable wind speed and wind direction. Further it should be
309   noted that for the days with successive NPF events, W_1 was chosen just before the initiation of nucleation event.
310   The second time window was selected when the GMD of aerosol particles was well above the 40 nm. Thus the
311   change in CCN concentration was calculated as:
312

313    $$\Delta CCN = \frac{CCN_{W_2} - CCN_{W_1}}{CCN_{W_1}}$$

314

Atmospheric
Chemistry
and Physics
Discussions

315   Table 2 gives the change in CCN concentration and other parameters for the 13 strong NPF events, which is

316   ~27% of all the events. These days are chosen on the basis of availability of all the simultaneous measurements

317   (aerosol chemical composition, PNC and meteorological parameters) and the fulfillment of the requirements for

318   the number concentration of strong events in section 4. The CCN measurements were selected at 0.52% SS in

319   this study, which would correspond to activation diameters around 70 nm for hygroscopic particles (Singla et

320   al., 2017). A considerable increase in CCN concentrations was observed after the event on each day with an

321   average increment of $42 \pm 27\%$ (Table 2). In this study, POA (primary organic aerosol) was also used as a

322   surrogate for BC (tracer for primary emission). The parameters - change in activated fraction and change in

323   CCN/POA, were calculated to identify the source of increased CCN concentrations. If the change in activated

324   fraction is similar to the change in CCN/POA, then primary emissions are the likely contributors for increased

325   CCN concentrations. On the other hand, if the change in activated fraction differs from the change in

326   CCN/POA, newly formed particles are the major contributors to increased CCN concentrations (de España et

327   al., 2017). It is observed from Table 2 that the change in activated fraction differs significantly from the change

328   in CCN/POA for each day. As an example, the metrics for 12th December shows that, the change in CCN/CN is

329   26% and the change in CCN/POA is -18%. This significant difference (between W1 and W2, refer figure 1)

330   indicated new particle formation as the important source of CCN at our site. The significant difference between

331   Δ(CCN/CN) and Δ(CCN/POA) for all the chosen events suggested NPF as the distinct source of increased

332   CCN. Further, Δ(CCN/NR-PM$_1$) was also calculated for accounting the BLH effect, if any. The positive change

333   of ΔCCN/NR-PM$_1$ indicated that higher CCN/NR-PM$_1$ after the event was the result of NPF and not the dilution

334   of BLH.

335

336   **4.4 Cluster analysis**

337   The cluster analysis was carried out to outline the relationship of air masses with the observed particle number

338   size distribution of aerosols. The trajectories were simulated by using the Hybrid Single-Particle Lagrangian

339   Integrated Trajectory (HYSPLIT) model (Draxler and Rolph, 2003). The 120 hour backward trajectories were

340   calculated for every hour terminating at a height of 100 m above the ground level. In total, 2760 trajectories

341   were calculated during the study period. The transport pathways of the observed air masses were grouped into

342   five clusters on the basis of total spatial variance (TSV). Each cluster congregated into different geographical

343   origin(s). The air-mass backward trajectory calculations and cluster analysis were performed by using Zefir

344   (Igor-based software developed by Petit et al., 2017). Before running the cluster analysis, backward trajectory

345   data was down-weighted by using the discrete weighting function in Zefir (Petit et al., 2017).

346

347   Figure 4(a) shows the derived fire hotspots (good indicators for biomass burning activities), from MODIS

348   (Moderate Resolution Imaging Spectro-radiometer) and geographical origin of each cluster and Figure 4(b)

349   shows the corresponding PNSD observed at the receptor site. The PNSD of each cluster was constructed by

350   averaging the particle number size distribution for each time step belonging to that particular cluster. It was

351   observed that air masses arriving at the receptor site generally originated from the inland continent and

352   represented 95% of the total back trajectories (cluster C1 - 51%, cluster C2 - 13% and cluster C3 - 25%). Cluster

353   C1 originated from Central India, C2 from northwest India and C3 from southeast India. On the other hand,

354   clusters C4 and C5 began from Iran and Saudi Arabia respectively and contributed only 4% and 7% respectively

355 to the total back trajectories. Before reaching the receptor site, cluster C4 traveled long through the land and

356 cluster C5 traveled both through the sea and land. Both the clusters - C4 and C5 were identified as fast moving

357 clusters. However, only cluster C4 was found to be a relatively cleaner air mass as the total NR-PM$_1$

358 concentration for C4 was found to be 7.2 µgm^{-3}. On the other hand, continental originated clusters were

359 identified as slow moving clusters and were associated with higher PM$_1$ concentration (C1 ~15 µgm^{-3}, C2 ~11

360 µgm^{-3} and C3 ~13 µgm^{-3}). The results of PNSD showed that the formation and growth of nucleation mode

361 particles were significant for clusters associated with continental air masses (Figure 4). Clusters (C4 and C5) did

362 not contain any nucleation although the mean total particle number concentration was comparable. The

363 characteristics of aerosol particles associated with each cluster were analyzed by dividing the PNC into 3

364 distinct modes - nucleation (5-25 nm), Aitken (25-100 nm) and accumulation (100-1000 nm) mode. The diurnal

365 variation of PNC in these 3 modes for each cluster is shown in Figure S2.

366

367 Nucleation mode - The particles in this mode showed significant increase in number concentration from 11:00

368 to 15:00 hours for clusters C1 and C2 with the considerable decrease in N$_{ait}$ concentration. This increase was

369 mainly influenced by the formation and growth of new particles under favourable meteorological conditions.

370 However, a faded increase in the number concentration was also observed for cluster C3 between 13:00 and

371 15:00 hours ~1155 cm^{-3}). This diminished nucleation was attributed to the interference caused by a sudden

372 increase in N$_{ait}$ concentration at the onset of nucleation. Thereafter, the nucleation event persisted for few hours.

373 Conversely, no nucleation process was observed for clusters C4 and C5. The diurnal variation of N$_{nuc}$ particles

374 exhibited high concentration during morning, afternoon and evening hours. However, these N$_{nuc}$ peaks

375 coincided well with the N$_{ait}$ concentration peaks. The simultaneous peaks in the two modes suggested the

376 emission of nucleation particles directly by local sources.

377

378 Aitken mode - For all the air mass cluster types, the particles in this mode reflected a morning (~08:00 hrs) and

379 an evening (~18:00 hrs) peak corresponding to traffic rush hours. In addition, clusters C3, C4 and C5 showed

380 somewhat elevated concentrations during afternoon and early evening in the PNC. These peaks may be

381 attributed to the fresh anthropogenic emissions by cooking related sources (Mukherjee et al., 2018). The mean

382 PNC during the morning peak was 2.5*10^3 cm^{-3}, 2.6*10^3 cm^{-3}, 2.4*10^3 cm^{-3}, 5.5*10^3 cm^{-3} and 5.2*10^3 cm^{-3} for

383 clusters C1, C2, C3, C4 and C5 respectively. In addition, a significant noon peak related to cooking was

384 observed for cluster C3 (~ 2663 cm^{-3}).

385

386 Accumulation mode - The PNC in this mode showed a stable pattern as a function of time for clusters C1, C2

387 and C3. This stable pattern of PNC indicated the regional transport of anthropogenic pollution to the receptor

388 site. The regional transport of organics and sulfate has been reported during the same period in our earlier work

389 (Mukherjee et al., 2018). The 24-hour average concentration of N$_{acc}$ particles was measured as 1.8*10^3 cm^{-3},

390 2.0*10^3 cm^{-3}, 1.8*10^3 cm^{-3}, 1.4*10^3 cm^{-3} and 2.1*10^3 cm^{-3} for clusters C1, C2, C3, C4 and C5 respectively.

391

392 The above analysis revealed that the clusters associated with continental air masses favoured new particle

393 formation under the influence of long range transported anthropogenic pollution to the sampling site. However,

394 the clusters associated with foreign air masses did not favour new particle formation. Based on the diurnal

395 variation of N_{nuc}, N_{ait} and N_{acc}, it was assumed that the concentration of N_{ait} is influencing the occurence of NPF.

396 It was noticed that the concentration of N_{ait} during the morning hours was well below ~$3*10^3$ cm^{-3} for

397 continental clusters and much above ~$5.5*10^3$ cm^{-3} for the foreign clusters. Also, the nucleation process was

398 found to be inhibited for cluster C3 by the sudden increase in N_{ait} concentration (~$2.7*10^3$ cm^{-3}) during the

399 afternoon hours. These statistics suggest that the number concentration of ~$3*10^3$ cm^{-3} may be acting as a

400 threshold value of N_{ait} particles for the appearance of NPF. The concentration of N_{ait} below ~$3*10^3$ cm^{-3} was

401 found to favour NPF at this site during the study period and vice versa. On the other hand, clusters 4 and 5 also

402 show a decrease in N_{ait} after the morning period, and still NPF does not take place. This may be indicative of

403 low addition of condensable vapours needed for NPF for the cluster 4 and 5 air masses, whereas it is likely that

404 the addition of condensable vapours for NPF is high enough in the Clusters 1-3. The insight into the relationship

405 between N_{ait} concentration and nucleation process was further comprehended by analyzing the individual days.

406 As an example, three days - 12th Dec 2016, 19th Dec 2016 and 19th Nov 2016 were chosen as representative days

407 for NPF, non NPF and weak NPF respectively. The selected days belongs to cluster C1. The cluster C1 was

408 chosen because it contributed most (~51%) to the total back trajectories.

409

410 Figure 5 shows the diurnal variation of PNC in 3 modes (N_{nuc}, N_{ait} and N_{acc}) for three selected days. The

411 variation in meteorology - temperature (T), relative humidity (RH) and wind speed (WS) is shown in Figure S3.

412 The PNC in the Aitken mode during 07:00 - 09:00 hrs was found to be ~$2.2*10^3$ cm^{-3}, ~$3.6*10^3$ cm^{-3} and

413 ~$2.6*10^3$ cm^{-3} on NPF, non-NPF and weak NPF day respectively for the three selected days. The variation of

414 solar radiation and temperature was found to be similar on all the days. On the other hand, RH varied

415 considerably. During the NPF day, the mean RH was ~36 ± 7 % with the minimum of ~23% during the

416 nucleation process. The non-NPF and weak NPF day showed a mean RH of ~57 ± 4% and ~26 ± 7%

417 respectively. The magnitude of WS was also variable. The NPF day, non-NPF day and weak NPF day showed

418 mean WS of 6.2 ± 2.8 ms^{-1}, 2.4 ± 1.2 ms^{-1} and 4.1 ± 1.6 ms^{-1}. Further, high WS was recorded just before the

419 nucleation event (08:00 to 09:00 hrs), ~8.7 ms^{-1} on the NPF day, ~1.7 ms^{-1} on the non-NPF day and 6.8 ms^{-1}

420 (10:00 hrs) on the weak NPF day. On the basis of these statistics, it was concluded that stable, relatively low

421 background Aitken mode concentrations with low RH favoured the new particle formation on 12th December

422 under high wind speed, temperature and solar radiation conditions. On the other hand, fresh anthropogenic

423 emissions and unfavourable meteorological conditions inhibited the nucleation activity on 19th December. The

424 fresh anthropogenic emissions were observed during morning (~$3.4*10^3$ cm^{-3}) and noon (~$3.1*10^3$ cm^{-3}) on 19th

425 November as well. However, the N_{ait} concentration was much lower than that observed on the non-NPF day.

426 Secondly, the molar ratio of ammonium to inorganic anions was calculated as ~1.4. Since both source

427 (ammonia) and sink (pre-existing particles due to fresh anthropogenic emissions) entities were present in high

428 amount, it was not likely inhibiting NPF as suggested in section 4.2. Instead, relatively unfavourable

429 meteorological conditions inhibited strong formation on the weak NPF event day. Moreover, the interference by

430 fresh emissions during noon time was assumed to suppress the nucleation activity and hence lead to the weak

431 NPF day with maximum N_{nuc} ~ $4.5*10^3$ cm^{-3} at 15:00 hrs.

432

433 Since the nucleation process in this study was influenced by the transported anthropogenic pollution, the

434 chemical composition of each cluster was also evaluated. Table 3 gives the mass concentration of organic and

435   inorganic components of aerosol particles. The comparable mass concentration of nitrate and HOA indicated no

436   influence of long range transport on NPF. The mass concentration of sulfate, ammonium, BBOA and OOA was

437   higher for the continental clusters 1-3 as compared to the foreign clusters 4-5. This difference may be attributed

438   to the travel pathways of each cluster. Clusters C4 and C5 were identified as fast moving clusters and had a

439   lower travel time over the continent. Therefore, it was assumed that high mass concentration of sulfate,

440   ammonium, BBOA and OOA were indicative of local or regional emissions. The continental clusters originated

441   from the biomass burning affected areas and identified to represent regional, or in other words, long range

442   transported aerosol particles (Figure 4). The higher mass concentration of BBOA was attributed to the regional

443   transport of biomass burning related aerosols. With a reported lifetime of 3.8 ± 0.8 days (Edwards et al., 2006),

444   biomass burning plumes are often transported for thousands of kilometers (Anderson et al., 1996; Andreae et al.,

445   1988). The higher mass concentration of sulfate was also related to long range transport. Since no direct

446   measurements of SO_2 were available at this site, the spatial distribution of SO_2 emissions over the Indian region

447   was extracted from the OMI satellite (Figure S4). Figure S4 shows high SO_2 emissions in central India. The

448   biomass burning events and power plants seems to serve as the two major sources of SO_2 emissions during the

449   study period (Figure 4 and S4). It is reported that NO_2 can act as an important oxidant for the conversion of SO_2

450   to sulfate under biomass burning influenced anthropogenic pollution (Xie et al., 2015). Further, the continental

451   clusters also displayed higher mass concentration of OOA. This high concentration was attributed to the

452   atmospheric changes in biomass burning aerosols often resulting in the enhanced fraction of OOA and

453   degradation of biomass burning related species (Cubison et al., 2011; DeCarlo et al., 2008; Yokelson et al.,

454   2009). Therefore, it can be concluded that the formation of new particles took place under the influence of

455   biomass burning affected anthropogenic pollution. The chamber study by Henningan et al., 2012 has shown that

456   exposing the biomass burning plume to UV light initiates photo-oxidation thereby creating a strong nucleation

457   burst. The field studies have also reported the nucleation activity in fresh (Hobbs et al., 2003) and aged fire

458   plumes (Andreae et al., 2001; Wu et al., 2016).

459

460   **4.5 NanoMap**

461   The NanoMap method (Kristensson et al., 2014) was used to identify the spatial distribution of NPF events

462   during the formation of 1.5 nm particle diameter. It is only applicable to the areas which are upwind and up to

463   500 km from the sampling site. This method helps in determining the spatial NPF events occurring at the same

464   time as at the sampling site. In this study, the dataset of 4 months (November 2016 to February 2017) was used

465   to earmark the source area and frequency of the formation of 1.5 nm diameter particles along the trajectories.

466   The data was available for 95% of total days (115 days out of 120 days). During these days, 34% of days (~40

467   days) were identified as type-I NPF event days. All the events were easily analyzable with respect to start time

468   of NPF and end of growth time.

469

470   Figure 6 shows the location of formation of 1.5 nm diameter upwind of the HACPL site with a grid resolution of

471   0.1 x 0.2°. A large NPF frequency was observed in the areas favoured solely by the continental air masses. The

472   biomass burning mixed anthropogenic plume from the Central India seems to favour the occurrence of the NPF

473   events upwind of HACPL. However, no NPF events were registered with the air masses coming from other

474   directions. The probable reason could be the non-availability of sufficient precursors (SO_2 or H_2SO_4) at the

475   sampling site. Figure S4 shows the SO_2 emission for the time period - November 2016 to February 2017. It has

476   been reported that SO_2 once emitted, readily reacts with hydroxyl radical in the atmosphere to produce SO_3. The

477   SO_3 formed then reacts quickly with water vapour to produce sulphuric acid or depending on the meteorological

478   conditions and availability of oxidizing substances; SO_2 may be transported hundreds of kilometres before it

479   forms sulfuric acid (Erduran and Tuncel, 2001). Another possibility is that the oxidation of trace gases emitted

480   from biomass burning produced low-volatile condensable vapours, which nucleated in the biomass burning

481   plume (Wu et al., 2016). Moreover, a recent study found that biomass burning can enhance the conversion of

482   NO_2 to HONO, which is one of the main sources of OH (Hobbs et al., 2003; Yokelson et al., 2009; Nie et al.,

483   2015). Therefore the biomass burning mixed anthropogenic plume was expected to transport ample amount of

484   precursor gases (SO_2 or H_2SO_4) initiating the nucleation upwind of the HACPL site. The spatial extension of the

485   NPF of 1.5 nm diameter particles extended up to several hundred kilometres from HACPL according to the

486   NanoMap method. In reality, the extension could be even higher than this. This is not possible to observe due to

487   sudden interruptions in the GR of newly formed particles during NPF, and the limitations of the NanoMap

488   method (Kristensson et al., 2014).

489

490   **Conclusion**

491   The simultaneous measurements of particle number size distribution, aerosol chemical composition and

492   meteorology were performed at Mahabaleshwar from November 2016 to February 2017. The data was analyzed

493   to identify the occurrence of nucleation events. Ample NPF events were observed with a frequency of ~40%.

494   Certain meteorological conditions were favourable during the study period for NPF, and local and long range

495   transported aerosol sources played a significant role in the occurrence of NPF. The main conclusions drawn

496   from this study are listed below:

497   (i) All the NPF events began around 10:00-11:00 hours. Ten of the strongest NPF events observed had an

498   average growth rate, formation rate, condensation sink and coagulation of 2.6 ± 0.4 nm h^{-1}, 2.8 ± 1.4 cm^{-3} s^{-1}, 2.2

499     $\pm 2.9 \times 10^{-2}$ s^{-1} and 1.6 ± 1.0 cm^{-3} s^{-1} respectively.

500   (ii) Fresh anthropogenic emissions (resulting in high N_{ait} concentration) or unfavourable meteorology led to

501   weak or no NPF events. On the basis of cluster analysis of backward trajectories, a concentration lower than

502   3×10^3 cm^{-3} was earmarked as the threshold value of Aitken mode particles favoring nucleation. During the non-

503   NPF event days N_{ait} concentrations were significantly higher.

504   (iii) The analysis suggested that (a) the air masses influenced by biomass burning fromnorth-east and (b) high

505   wind speed just before the nucleation event favored nucleation at HACPL.

506   (iv) The growth of freshly nucleated particles persisted for ~ 6-7 hours and led to the significant enhancement in

507   mass concentration of aerosol (OOA, sulfate and nitrate).

508   (v) The NPF events acted as the significant source of CCN with the mean percentage increment of ~53 ± 36%.

509   (vi) NPF took place up to several hundred kilometers upwind to the north-east of HACPL.

510

511   **Data availability**

512   The data used in this study are from the data repository of HACPL, part of IITM, Pune and will be made

513   available on request.

514

Atmospheric
Chemistry
and Physics
Discussions

522

523 **Competing interests**

524 The authors declare that they have no conflict of interest.

525

526 **References**

527 Anderson, B. E., Grant, W. B., Gregory, G. L., Browell, E. V., Collins, J. E., Sachse, G. W., Bagwell, D. R.,

528 Hudgins, C. H., Blake, D. R. and Blake, N. J.: Aerosols from biomass burning over the tropical South

529 Atlantic region: Distributions and impacts, J. Geophys. Res. Atmos., 101(D19), 24117–24137,

530 doi:10.1029/96JD00717, 1996.

531 Andreae, M. O., Artaxo, P., Fischer, H., Freitas, S. R., Grégoire, J. M., Hansel, A., Hoor, P., Kormann, R.,

532 Krejci, R., Lange, L., Lelieveld, J., Lindinger, W., Longo, K., Peters, W., De Reus, M., Scheeren, B., Silva

533 Dias, M. A. F., Ström, J., Van Velthoven, P. F. J. and Williams, J.: Transport of biomass burning smoke to

534 the upper troposphere by deep convection in the equatorial region, Geophys. Res. Lett., 28(6), 951–954,

535 doi:10.1029/2000GL012391, 2001.

536 Andreae, M.O., Browell, E.V., Garstang, M., Gregory, G.L., Harriss, R.C., Hill, G.F., Jacob, D.J., Pereira,

537 M.C., Sachse, G.W., Setzer, A.W. and Dias, P.L.: Biomass-burning emissions and associated haze layers

538 over Amazonia. J. Geophys. Res. Atmos., 93(D2), pp.1509-1527,

539 doi:https://doi.org/10.1029/JD093iD02p01509, 1988.

540 Barsanti, K. C., McMurry, P. H. and Smith, J. N.: The potential contribution of organic salts to new particle

541 growth, Atmos. Chem. Phys., 9(9), 2949–2957 doi: https://doi.org/10.5194/acp-9-2949-2009, 2009.

542 Creamean, J. M., Ault, A. P., Ten Hoeve, J. E., Jacobson, M. Z., Roberts, G. C., Prather, K. A., Hoeve, J. E.

543 Ten, Jacobson, Z., Roberts, G. C. and Prather, K. A.: Measurements of Aerosol Chemistry during New

544 Particle Formation Events at a Remote Rural Mountain Site Centre National de Recherches

545 Météorologiques – Groupe, Environ. Sci. Technol., 45(19), 8208–8216, doi:10.1021/es103692f, 2011.

546 Crilley, L. R., Jayaratne, E. R., Ayoko, G. A., Miljevic, B., Ristovski, Z. and Morawska, L.: Observations

547 on the Formation, Growth and Chemical Composition of Aerosols in an Urban Environment, Environ.Sci.

548 Technol., 48, 6588–6596, doi:10.1021/es5019509, 2014.

549 Cubison, M. J., Ortega, A. M., Hayes, P. L., Farmer, D. K., Day, D., Lechner, M. J., Brune, W. H., Apel, E.,

550 Diskin, G. S., Fisher, J. A., Fuelberg, H. E., Hecobian, A., Knapp, D. J., Mikoviny, T., Riemer, D., Sachse,

551 G. W., Sessions, W., Weber, R. J., Weinheimer, A. J., Wisthaler, A. and Jimenez, J. L.: Effects of aging on

552   organic aerosol from open biomass burning smoke in aircraft and laboratory studies, Atmos. Chem. Phys.,
553   11(23), 12049–12064, doi:10.5194/acp-11-12049-2011, 2011.

554   Dal Maso, M.: Formation and Growth of Fresh Atmospheric Aerosols Eight Years of Aerosol Size
555   Distribution Data From SMEAR, Boreal Environ. Res., 10(October 2005), 323–336, 2005.

556   Dameto de España, C., Wonaschütz, A., Steiner, G., Rosati, B., Demattio, A., Schuh, H. and Hitzenberger,
557   R.: Long-term quantitative field study of New Particle Formation (NPF) events as a source of Cloud
558   Condensation Nuclei (CCN) in the urban background of Vienna, Atmos. Environ., 164, 289–298,
559   doi:10.1016/j.atmosenv.2017.06.001, 2017.

560   DeCarlo, P. F., Dunlea, E. J., Kimmel, J. R., Aiken, A. C., Sueper, D., Crounse, J., Wennberg, P. O.,
561   Emmons, L., Shinozuka, Y., Clarke, A., Zhou, J., Tomlinson, J., Collins, D. R., Knapp, D., Weinheimer, A.
562   J., Montzka, D. D., Campos, T. and Jimenez, J. L.: Fast airborne aerosol size and chemistry measurements
563   above Mexico City and Central Mexico during the MILAGRO campaign, Atmos. Chem. Phys., 8(14),
564   4027–4048, doi:10.5194/acp-8-4027-2008, 2008.

565   Draxler, R.R. and Rolph, G.D., 2003. HYSPLIT (HYbrid single-particle Lagrangian integrated trajectory)
566   model access via NOAA ARL READY. NOAA Air Resources Laboratory, Silver Spring, MD.
567   Dostupnona: http://ready. arl. noaa. gov/HYSPLIT. php (06. 06. 2010.).

569   Dusek, U., Frank, G. P., Hildebrandt, L., Curtius, J., Schneider, J., Walter, S., Chand, D., Drewnick, F.,
570   Hings, S., Jung, D., Borrmann, S. and Andreae, M. O.: Size Matters More Than Chemistry Aerosol
571   Particles, Science, 312(5778), 1375–1378, doi:10.1126/science.1125261, 2006.

572   Edwards, D. P., Emmons, L. K., Gille, J. C., Chu, A., Attié, J. L., Giglio, L., Wood, S. W., Haywood, J.,
573   Deeter, M. N., Massie, S. T., Ziskin, D. C. and Drummond, J. R.: Satellite-observed pollution from
574   Southern   Hemisphere   biomass   burning,   J.   Geophys.   Res.   Atmos.,   111(14),   1–17,
575   doi:10.1029/2005JD006655, 2006.

576   Engelhart, G. J., Hildebrandt, L., Kostenidou, E., Mihalopoulos, N., Donahue, N. M. and Pandis, S. N.:
577   Water content of aged aerosol, Atmos. Chem. Phys., 11(3), 911–920, doi:10.5194/acp-11-911-2011, 2011.

578   Erduran, M.S. and Tuncel, S.G.: Gaseous and particulate air pollutants in the Northeastern Mediterranean
579   Coast. Science of the total environment, 281(1-3), pp.205-215, doi:https://doi.org/10.1016/S0048-
580   9697(01)00847-6, 2001.

581   Fan, J., Rosenfeld, D., Ding, Y., Leung, L. R. and Li, Z.: Potential aerosol indirect effects on atmospheric
582   circulation and radiative forcing through deep convection, Geophys. Res. Lett., 39(9), 1–7,
583   doi:10.1029/2012GL051851, 2012.

584   Fiore, A. M., Naik, V., Spracklen, D. V., Steiner, A., Unger, N., Prather, M., Bergmann, D., Cameron-
585   Smith, P. J., Cionni, I., Collins, W. J., Dalsoren, S., Eyring, V., Folberth, G. A., Ginoux, P., Horowitz, L.
586   W., Josse, B., Lamarque, J. F., MacKenzie, I. A., Nagashima, T., O'Connor, F. M., Righi, M., Rumbold, S.

587   T., Shindell, D. T., Skeie, R. B., Sudo, K., Szopa, S., Takemura, T. and Zeng, G.: Global air quality and
588   climate, Chem. Soc. Rev., 41(19), 6663–6683, doi:10.1039/c2cs35095e, 2012.

589   Gong, Y., Su, H., Cheng, Y., Liu, F., Wu, Z., Hu, M., Zeng, L. and Zhang, Y.: Analysis on concentration
590   and source rate of precursor vapors participating in particle formation and growth at xinken in the Pearl
591   River Delta of China, Adv. Atmos. Sci., 25(3), 427–436, doi:10.1007/s00376-008-0427-4, 2008.

592   Gong, Y., Hu, M., Cheng, Y., Su, H., Yue, D., Liu, F., Wiedensohler, A., Wang, Z., Kalesse, H., Liu, S.,
593   Wu, Z., Xiao, K., Mi, P. and Zhang, Y.: Competition of coagulation sink and source rate: New particle
594   formation in the Pearl River Delta of China, Atmos. Environ., 44(27), 3278–3285,
595   doi:10.1016/j.atmosenv.2010.05.049, 2010.

596   Hamed, A., Korhonen, H., Sihto, S. L., Joutsensaari, J., Jrvinen, H., Petäjä, T., Arnold, F., Nieminen, T.,
597   Kulmala, M., Smith, J. N., Lehtinen, K. E. J. and Laaksonen, A.: The role of relative humidity in
598   continental new particle formation, J. Geophys. Res. Atmos., 116(3), 1–12, doi:10.1029/2010JD014186,
599   2011.

600   Hennigan, C. J., Westervelt, D. M., Riipinen, I., Engelhart, G. J., Lee, T., Collett, J. L., Pandis, S. N.,
601   Adams, P. J. and Robinson, A. L.: New particle formation and growth in biomass burning plumes: An
602   important source of cloud condensation nuclei, Geophys. Res. Lett., 39(9), 1–5,
603   doi:10.1029/2012GL050930, 2012.

604   Hobbs, P. V., Sinha, P., Yokelson, R. J., Christian, T. J., Blake, D. R., Gao, S., Kirchstetter, T. W.,
605   Novakov, T. and Pilewskie, P.: Evolution of gases and particles from a savanna fire in South Africa, J.
606   Geophys. Res. Atmos., 108(D13), n/a-n/a, doi:10.1029/2002JD002352, 2003.

607   Kanawade, V. P., Tripathi, S. N., Siingh, D., Gautam, A. S., Srivastava, A. K., Kamra, A. K., Soni, V. K.
608   and Sethi, V.: Observations of new particle formation at two distinct Indian subcontinental urban locations,
609   Atmos. Environ., 96, 370–379, doi:10.1016/j.atmosenv.2014.08.001, 2014.

610   Kerminen, V. M. and Kulmala, M.: Analytical formulae connecting the "real" and the "apparent"
611   nucleation rate and the nuclei number concentration for atmospheric nucleation events, J. Aerosol Sci.,
612   33(4), 609–622, doi:10.1016/S0021-8502(01)00194-X, 2002.

613   Kerminen, V. M., Paramonov, M., Anttila, T., Riipinen, I., Fountoukis, C., Korhonen, H., Asmi, E., Laakso,
614   L., Lihavainen, H., Swietlicki, E., Svenningsson, B., Asmi, A., Pandis, S. N., Kulmala, M. and Petäjä, T.:
615   Cloud condensation nuclei production associated with atmospheric nucleation: A synthesis based on
616   existing literature and new results, Atmos. Chem. Phys., 12(24), 12037–12059, doi:10.5194/acp-12-12037-
617   2012, 2012.

618   Kivekäs, N., Carpman, J., Roldin, P., Leppä, J., O'Connor, E., Kristensson, A. and Asmi, E.: Coupling an
619   aerosol box model with one-dimensional flow: A tool for understanding observations of new particle
620   formation events, Tellus, Ser. B Chem. Phys. Meteorol., 68(1), doi:10.3402/tellusb.v68.29706, 2016.

621   Kristensson, A., Johansson, M., Swietlicki, E., Kivekäs, N., Hussein, T., Nieminen, T. and Kulmala, M.:
622   NanoMap : Geographical mapping of atmospheric new- particle formation through analysis of particle
623   number size distribution and trajectory data, , 19(September), 329–342, 2014.

624   Kulmala, M. and Kerminen, V. M.: On the formation and growth of atmospheric nanoparticles, Atmos.
625   Res., 90(2–4), 132–150, doi:10.1016/j.atmosres.2008.01.005, 2008.

626   Kulmala, M., Kontkanen, J., Junninen, H., Lehtipalo, K., Manninen, H. E., Nieminen, T., Petäjä, T., Sipilä,
627   M., Schobesberger, S., Rantala, P., Franchin, A., Jokinen, T., Järvinen, E., Äijälä, M., Kangasluoma, J.,
628   Hakala, J., Aalto, P. P., Paasonen, P., Mikkilä, J., Vanhanen, J., Aalto, J., Hakola, H., Makkonen, U.,
629   Ruuskanen, T., Mauldin, R. L., Duplissy, J., Vehkamäki, H., Bäck, J., Kortelainen, A., Riipinen, I., Kurtén,
630   T., Johnston, M. V., Smith, J. N., Ehn, M., Mentel, T. F., Lehtinen, K. E. J., Laaksonen, A., Kerminen, V.
631   M. and Worsnop, D. R.: Direct observations of atmospheric aerosol nucleation, Science, 339(6122), 943–
632   946, doi:10.1126/science.1227385, 2013.

633   Kulmala, M., Vehkamäki, H., Petäjä, T., Dal Maso, M., Lauri, A., Kerminen, V. M., Birmili, W. and
634   McMurry, P. H.: Formation and growth rates of ultrafine atmospheric particles: A review of observations, J.
635   Aerosol Sci., 35(2), 143–176, doi:10.1016/j.jaerosci.2003.10.003, 2004.

636   Lance, S., Medina, J., Smith, J. and Nenes, A.: Mapping the operation of the DMT continuous flow CCN
637   counter, Aerosol Sci. Technol., 40(4), 242–254, doi:10.1080/02786820500543290, 2006.

638   Leena, P. P., Anil Kumar, V., Dani, K. K., Sombawne, S. M., Murugavel, P. and Pandithurai, G.: Evidence
639   of new particle formation during post monsoon season over a high-altitude site of the Western Ghats, India,
640   Toxicol. Environ. Chem., 99(4), 652–664, doi:10.1080/02772248.2016.1274031, 2017.

641   Levin, E., Prenni, a, Petters, M., Kreidenweis, S., Sullivan, R., Atwood, S., Ortega, J., Demott, P. and
642   Smith, J.: An annual cycle of size-resolved aerosol hygroscopicity at a forested site in Colorado, J.
643   Geophys. Res., 117(D6), D06201, doi:10.1029/2011JD016854, 2012.

644   Li, Y., Zhang, F., Li, Z., Sun, L., Wang, Z., Li, P., Sun, Y., Ren, J., Wang, Y., Cribb, M. and Yuan, C.:
645   Influences of aerosol physiochemical properties and new particle formation on CCN activity from
646   observation at a suburban site of China, Atmos. Res., 188, 80–89, doi:10.1016/j.atmosres.2017.01.009,
647   2017.

648   Lihavainen, H.: Production of "potential" cloud condensation nuclei associated with atmospheric new-
649   particle formation in northern Finland, J. Geophys. Res., 108, 1–8, doi:10.1029/2003JD003887, 2003.

650   Ma, N., Zhao, C., Tao, J., Wu, Z., Kecorius, S., Wang, Z., Groß, J., Liu, H., Bian, Y., Kuang, Y., Teich, M.,
651   Spindler, G., Muller, K., Van Pinxteren, D., Herrmann, H., Hu, M. and Wiedensohler, A.: Variation of CCN
652   activity during new particle formation events in the North China Plain, Atmos. Chem. Phys., 16(13), 8593–
653   8607, doi:10.5194/acp-16-8593-2016, 2016.

654   Mukherjee, S., Singla, V., Pandithurai, G., Safai, P. D., Meena, G. S., Dani, K. K. and Anil Kumar, V.:

655   Seasonal variability in chemical composition and source apportionment of sub-micron aerosol over a high
656   altitude site in Western Ghats, India, Atmos. Environ., 180(February), 79–92,
657   doi:10.1016/j.atmosenv.2018.02.048, 2018.

658   Németh, Z. and Salma, I.: Spatial extension of nucleating air masses in the Carpathian Basin, Atmos. Chem.
659   Phys., 14(16), 8841–8848, doi:10.5194/acp-14-8841-2014, 2014.

660   Nie, W., Ding, A. J., Xie, Y. N., Xu, Z., Mao, H., Kerminen, V. M., Zheng, L. F., Qi, X. M., Huang, X.,
661   Yang, X. Q., Sun, J. N., Herrmann, E., Petäjä, T., Kulmala, M. and Fu, C. B.: Influence of biomass burning
662   plumes on HONO chemistry in eastern China, Atmos. Chem. Phys., 15(3), 1147–1159, doi:10.5194/acp-15-
663   1147-2015, 2015.

664   Paatero, P. and Tapper, U.: Positive matrix factorization: A non???negative factor model with optimal
665   utilization of error estimates of data values, Environmetrics, 5(2), 111–126, doi:10.1002/env.3170050203,
666   1994.

667   Petit, J. E., Favez, O., Albinet, A. and Canonaco, F.: A user-friendly tool for comprehensive evaluation of
668   the geographical origins of atmospheric pollution: Wind and trajectory analyses, Environ. Model. Softw.,
669   88, 183–187, doi:10.1016/j.envsoft.2016.11.022, 2017.

670   Pierce, J. R. and Adams, P. J.: Uncertainty in global CCN concentrations from uncertain aerosol nucleation
671   and primary emission rates, Atmos. Chem. Phys., 9(4), 1339–1356, doi:10.5194/acp-9-1339-2009, 2009.

672   Pikridas, M., Riipinen, I., Hildebrandt, L., Kostenidou, E., Manninen, H., Mihalopoulos, N., Kalivitis, N.,
673   Burkhart, J. F., Stohl, A., Kulmala, M. and Pandis, S. N.: New particle formation at a remote site in the
674   eastern Mediterranean, J. Geophys. Res. Atmos., 117(12), 1–14, doi:10.1029/2012JD017570, 2012.

675   Riipinen, I., Sihto, S., Kulmala, M., Arnold, F., Maso, M. D., Birmili, W., Saarnio, K. and Teinil, K.:
676   Connections between atmospheric sulphuric acid and new particle formation during QUEST III – IV
677   campaigns in Heidelberg and Hyytiala, Atmos. Chem. Phys., 7, 1899–1914, doi:10.5194/acpd-6-10837-
678   2006, 2007.

679   Roberts, G. C. and Nenes, A.: A continuous-flow streamwise thermal-gradient CCN chamber for
680   atmospheric measurements, Aerosol Sci. Technol., 39(3), 206–221, doi:10.1080/027868290913988, 2005.

681   Rose, D., Nowak, A., Achtert, P., Wiedensohler, A., Hu, M., Shao, M., Zhang, Y., Andreae, M. O. and
682   Pöschl, U.: Cloud condensation nuclei in polluted air and biomass burning smoke near the mega-city
683   Guangzhou, China - Part 1: Size-resolved measurements and implications for the modeling of aerosol
684   particle hygroscopicity and CCN activity, Atmos. Chem. Phys., 10(7), 3365–3383, doi:10.5194/acp-10-
685   3365-2010, 2010.

686   Rosenfeld, D., Lohmann, U., Raga, G. B., O'Dowd, C. D., Kulmala, M., Fuzzi, S., Reissell, A. and
687   Andreae, M. O.: Flood or drought: How do aerosols affect precipitation?, Science, 321(5894), 1309–1313,
688   doi:10.1126/science.1160606, 2008.

Atmospheric
Chemistry
and Physics
Discussions

689   Seaton, A. and Dennekamp, M.: Hypothesis: Ill health associated with low concentrations of nitrogen
690   dioxide—an effect of ultrafine particles? Thorax, 58(12), 1012–1015.
691   http://doi.org/10.1136/thorax.58.12.1012, 2003.

692   See, S. W., Balasubramanian, R. and Wang, W.: A study of the physical, chemical, and optical properties of
693   ambient aerosol particles in Southeast Asia during hazy and nonhazy days, J. Geophys. Res. Atmos.,
694   111(10), 1–12, doi:10.1029/2005JD006180, 2006.

695   Shen, X., Sun, J., Kivekäs, N., Kristensson, A., Zhang, X., Zhang, Y., Zhang, L., Fan, R., Qi, X., Ma, Q.
696   and Zhou, H.: Spatial distribution and occurrence probability of regional new particle formation events in
697   eastern China, Atmos. Chem. Phys., 18(2), 587–599, doi:10.5194/acp-18-587-2018, 2018.

698   Singla, V., Mukherjee, S., Safai, P. D., Meena, G. S., Dani, K. K. and Pandithurai, G.: Role of organic
699   aerosols in CCN activation and closure over a rural background site in Western Ghats, India, Atmos.
700   Environ., 158, 148–159, doi:10.1016/j.atmosenv.2017.03.037, 2017.

701   Skrabalova, L., Zikova, N. and Zdimal, V.: Shrinkage of newly formed particles in an urban environment,
702   Aerosol Air Qual. Res., 15(4), 1313–1324, doi:10.4209/aaqr.2015.01.0015, 2015.

703   Spracklen, D. V., Carslaw, K. S., Kulmala, M., Kerminen, V. M., Sihto, S. L., Riipinen, I., Merikanto, J.,
704   Mann, G. W., Chipperfield, M. P., Wiedensohler, A., Birmili, W. and Lihavainen, H.: Contribution of
705   particle formation to global cloud condensation nuclei concentrations, Geophys. Res. Lett., 35(6), 1–5,
706   doi:10.1029/2007GL033038, 2008.

707   Stanier, C. O., Khlystov, A. Y. and Pandis, S. N.: Nucleation events during the Pittsburgh Air Quality
708   Study: Description and relation to key meteorological, gas phase, and aerosol parameters, Aerosol Sci.
709   Technol., 38(SUPPL. 1), 253–264, doi:10.1080/02786820390229570, 2004.

710   Stier, P., Seinfeld, J. H., Kinne, S. and Boucher, O.: Aerosol absorption and radiative forcing, Atmos.
711   Chem. Phys., 7(19), 5237–5261, doi:10.5194/acp-7-5237-2007, 2007.

712   Väänänen, R., Krejci, R., Manninen, H. E., Manninen, A., Lampilahti, J., Buenrostro Mazon, S., Nieminen,
713   T., Yli-Juuti, T., Kontkanen, J., Asmi, A., Aalto, P. P., Keronen, P., Pohja, T., O'Connor, E.,
714   Kerminen, V.-M., Petäjä, T. and Kulmala, M.: Vertical and horizontal variation of aerosol number size
715   distribution in the boreal environment, Atmos. Chem. Phys. Discuss., (July), 1–43, doi:10.5194/acp-2016-
716   556, 2016.

717   Vehkamäki, H. and Riipinen, I.: Thermodynamics and kinetics of atmospheric aerosol particle formation
718   and growth, Chem. Soc. Rev., 41(15), 5160–5173, doi:10.1039/c2cs00002d, 2012.

719   Wang, Z. B., Hu, M., Sun, J. Y., Wu, Z. J., Yue, D. L., Shen, X. J., Zhang, Y. M., Pei, X. Y., Cheng, Y. F.
720   and Wiedensohler, A.: Characteristics of regional new particle formation in urban and regional background
721   environments in the North China Plain, Atmos. Chem. Phys., 13(24), 12495–12506, doi:10.5194/acp-13-
722   12495-2013, 2013.

Atmospheric
Chemistry
and Physics
Discussions

723   Wiedensohler, A., Cheng, Y. F., Nowak, A., Wehner, B., Achtelt, P., Berghof, M., Birmili, W., Wu, Z. J.,
724   Hu, M., Zhu, T., Takegawa, N., Kita, K., Kondo, Y., Lou, S. R., Hofeumahaus, A., Holland, F., Wahner, A.,
725   Gunthe, S. S., Rose, D., Su, H. and Pöschl, U.: Rapid aerosol particle growth and increase of cloud
726   condensation nucleus activity by secondary aerosol formation and condensation: A case study for regional
727   air pollution in northeastern China, J. Geophys. Res. Atmos., 114(8), 1–13, doi:10.1029/2008JD010884,
728   2009.

729   Wu, Z., Hu, M., Liu, S., Wehner, B., Bauer, S., Ma ßLing, A., Wiedensohler, A., Petäjä, T., Dal Maso, M.
730   and Kulmala, M.: New particle formation in Beijing, China: Statistical analysis of a 1-year data set, J.
731   Geophys. Res. Atmos., 112(9), 1–10, doi:10.1029/2006JD007406, 2007.

732   Wu, Z., Zheng, J., Wang, Y., Shang, D., Du, Z., Zhang, Y. and Hu, M.: Chemical and physical properties of
733   biomass burning aerosols and their CCN activity: A case study in Beijing, China, Sci. Total Environ., 579,
734   1260–1268, doi:10.1016/j.scitotenv.2016.11.112, 2017.

735   Xie, Y., Ding, A., Nie, W., Mao, H., Qi, X., Huang, X., Xu, Z., Kerminen, V. M., Petäjä, T., Chi, X.,
736   Virkkula, A., Boy, M., Xue, L., Guo, J., Sun, J., Yang, X., Kulmala, M. and Fu, C.: Enhanced sulfate
737   formation by nitrogen dioxide: Implications from in-situ observations at the SORPES station, J. Geophys.
738   Res., 120(24), 12,679-12,694, doi:10.1002/2015JD023607, 2015.

739   Yokelson, R. J., Crounse, J. D., DeCarlo, P. F., Karl, T., Urbanski, S., Atlas, E., Campos, T., Shinozuka, Y.,
740   Kapustin, V., Clarke, A. D., Weinheimer, A., Knapp, D. J., Montzka, D. D., Holloway, J., Weibring, P.,
741   Flocke, F., Zheng, W., Toohey, D., Wennberg, P. O., Wiedinmyer, C., Mauldin, L., Fried, A., Richter, D.,
742   Walega, J., Jimenez, J. L., Adachi, K., Buseck, P. R., Hall, S. R. and Shetter, R.: Emissions from biomass
743   burning in the Yucatan, Atmos. Chem. Phys., 9(15), 5785–5812, doi:10.5194/acp-9-5785-2009, 2009.

744   Yue, D., Hu, M., Wu, Z., Wang, Z., Guo, S., Wehner, B., Nowak, A., Achtert, P., Wiedensohler, A., Jung,
745   J., Kim, Y. J. and Liu, S.: Characteristics of aerosol size distributions and new particle formation in the
746   summer in Beijing, J. Geophys. Res. Atmos., 114(14), 1–13, doi:10.1029/2008JD010894, 2009.

747   Yue, D. L., Hu, M., Zhang, R. Y., Wang, Z. B., Zheng, J., Wu, Z. J., Wiedensohler, A., He, L. Y., Huang,
748   X. F. and Zhu, T.: The roles of sulfuric acid in new particle formation and growth in the mega-city of
749   Beijing, Atmos. Chem. Phys., 10(10), 4953–4960, doi:10.5194/acp-10-4953-2010, 2010.

750   Yue, D. L., Hu, M., Zhang, R. Y., Wu, Z. J., Su, H., Wang, Z. B., Peng, J. F., He, L. Y., Huang, X. F.,
751   Gong, Y. G. and Wiedensohler, A.: Potential contribution of new particle formation to cloud condensation
752   nuclei in Beijing, Atmos. Environ., 45(33), 6070–6077, doi:10.1016/j.atmosenv.2011.07.037, 2011.

753   Zhang, Q., Stanier, C. O., Canagaratna, M. R., Jayne, J. T., Worsnop, D. R., Pandis, S. N. and Jimenez, J.
754   L.: Insights into the chemistry of new particle formation and growth events in Pittsburgh based on aerosol
755   mass spectrometry, Environ. Sci. Technol., 38(18), 4797–4809, doi:Doi 10.1021/Es035417u, 2004.

756
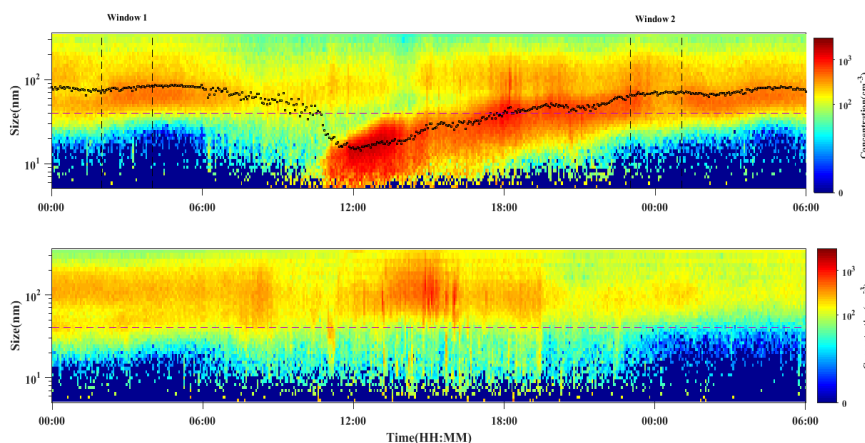
757

758   Figure 1: The spectrum of the particle number size distribution on a strong NPF day - 12th December 2016
759   (upper panel) and a non-NPF day - 14th December 2016 (lower panel). Window 1 and Window 2 represents the
760   stable atmospheric conditions before and after the nucleation started, respectively. The black dotted line in the
761   upper panel represents the geometric mean diameter of particles. The horizontal dashed line in both the panels
762   represents the diameter of particles at 40 nm.

763
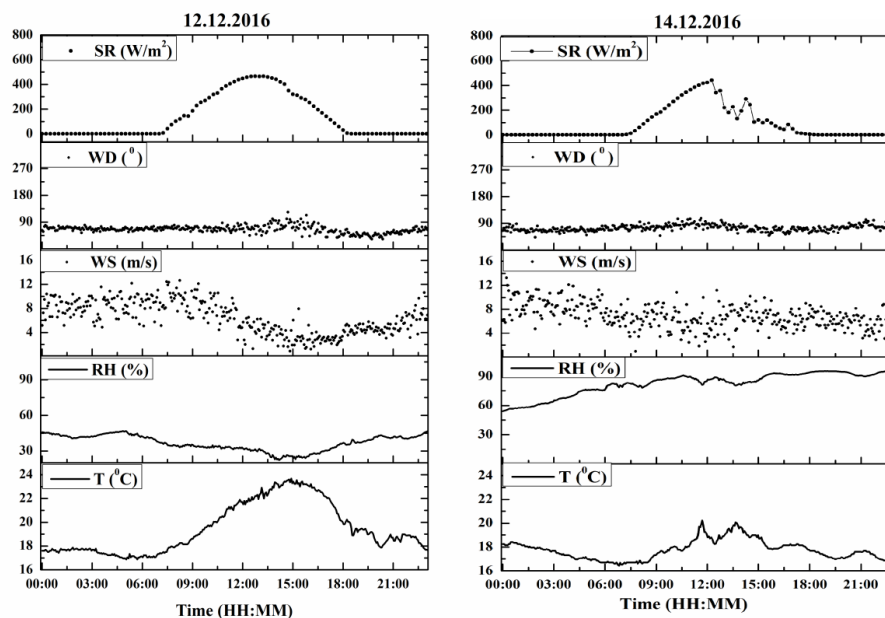
764

765   Figure 2: Diurnal variation of meteorological conditions - Solar radiation (SR), Wind direction (WD), Wind
766   speed (WS), Relative Humidity (RH) and Temperature (T) on the special case NPF day (left panel, December
767   12, 2016) and the non-NPF day (right panel, December 14, 2016).
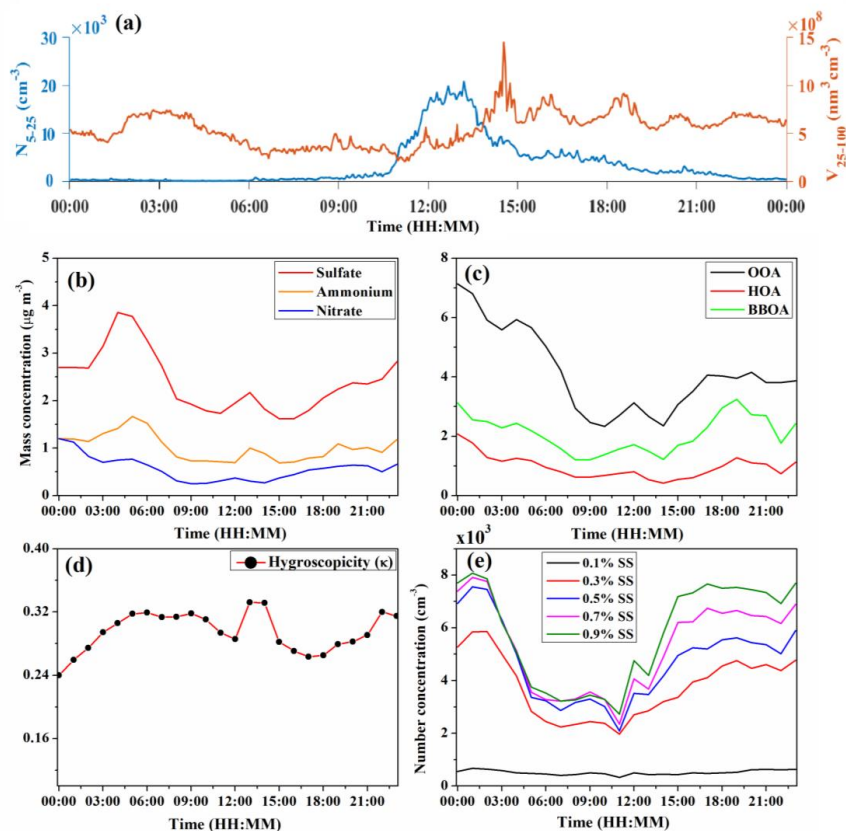
Figure 3: Particle properties during the strong NPF event day on December 12, 2016. Diurnal Variation of (a) nucleation mode number concentration and aitken mode volume concentration (b) mass concentration of secondary inorganic aerosol species (c) mass concentration of secondary organic aerosol species (OOA = oxygenated organic aerosol, HOA = hydrogenated organic aerosol, BBOA = biomass burning organic aerosol) (d) calculated hygroscopicity and (e) CCN number concentration at five supersaturations - 0.1%, 0.3%, 0.5%, 0.7% and 0.9%.
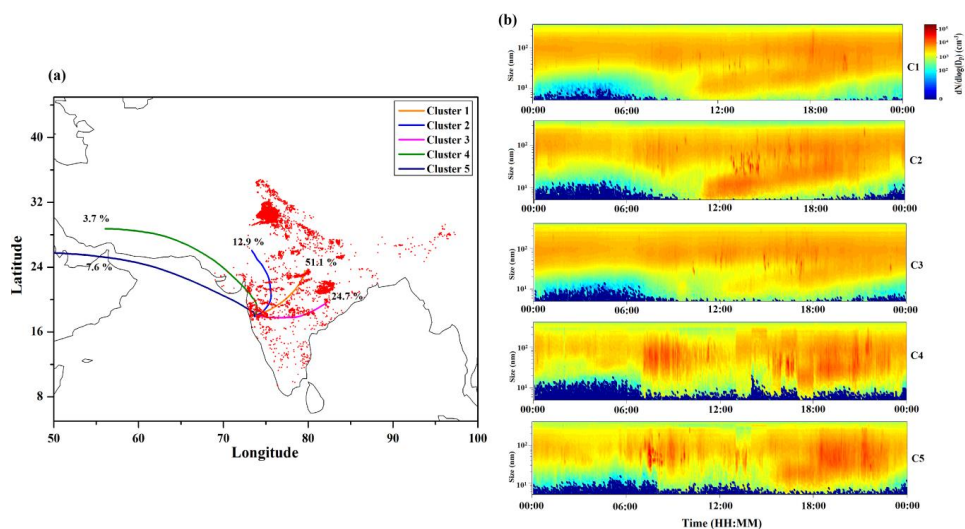
Atmospheric
Chemistry
and Physics
Discussions


780

Figure 4: Results of 120 h air mass backward trajectories at 100m above ground level during the study period (November 2016 to February 2017). Left Panel (a) - The mean trajectories of each cluster obtained through cluster analysis. Red dots represent the fire hotspots as identified by MODIS. Right Panel (b) - The spectrum of average particle number size distribution corresponding to each mean cluster.

785

786

787

788
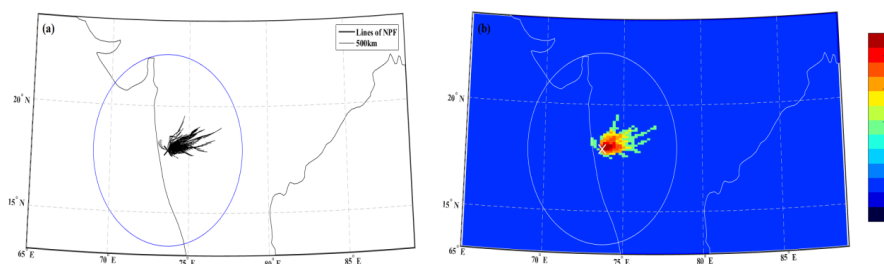

789

790
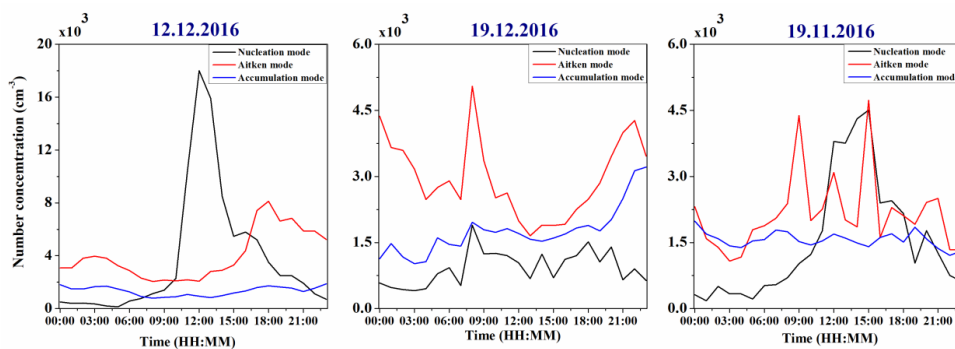
Figure 5: Diurnal Variation of particle number concentration in three modes - nucleation, aitken and accumulation mode for a NPF day -12th December 2016, a non-NPF day - 19th December 2016 and a weak-NPF day - 19th November 2016.

794

795

Figure 6: NanoMap results: Left Panel (a) - Black Lines represent the formation of 1.5 nm diameter particles. Right Panel (b) - The frequency of NPF events at 1.5 nm diameter, with a grid resolution of 0.1 x 0.2 degrees for latitude and longitude, respectively. The blue and white ovals limit the horizontal dimension of 500 km radius from the sampling site.

Atmospheric
Chemistry
and Physics
Discussions

820 Table 1: Summary of new particle formation events (strong event days) observed during November
821 2016 to February 2017. The start and end time were identified based on the change in GMD of
822 nucleation mode particles. The F_{coag} and J_5 were calculated at the time of NPF formation. The CS
823 corresponds to the time period ~1 hour before the start of NPF at 5.14 nm diameter. The GMD of
824 nucleation mode particles (5-25 nm) was used to calculate the GR.

Date	Start Time	End Time	J_5 (cm^{-3} s^{-1})	F_{coag} (cm^{-3} s^{-1})	CS (* 10^{-2} s^{-1})	GR$_{5-25}$ (nm h^{-1})
NPF Days						
8 Nov	11:00	18:00	4.9	3.4	2.1	2.3
9 Nov	10:00	17:00	6.6	5.2	2.0	2.4
10 Nov	11:00	17:00	6.9	5.4	2.2	2.4
12 Nov	11:00	17:00	3.9	3.0	2.3	2.5
18 Nov	10:00	16:00	7.3	6.3	2.2	3.3
2 Dec	10:00	17:00	2.0	1.5	2.1	2.2
12 Dec	11:00	18:00	6.6	5.1	2.0	2.5
13 Dec	10:00	16:00	5.2	4.4	2.9	2.3
17 Feb	12:00	18:00	2.4	1.8	2.1	3.0
18 Feb	11:00	18:00	4.1	3.3	2.5	2.9
Non-NPF Days						
14 Dec	-		-	-	4.4	-
15 Dec	-		-	-	4.2	-

825

826

827 Table 2: Summary of NPF event days qualifying the criterion mentioned in section 4.3. POA here
828 refers to the sum of HOA and BBOA. The information on HOA and BBOA was obtained by using
829 Positive Matrix Factorization. All the parameters listed below are calculated at 0.52% SS.

Date	ΔCCN	ΔCCN/CN	ΔCCN/POA	ΔCCN/NR-PM$_1$
07.11.16	40 %	24 %	61 %	99 %
08.11.16	29 %	37 %	65 %	44 %
09.11.16	43 %	45 %	77 %	23 %
10.11.16	19 %	15 %	32 %	11 %
18.11.16	21 %	34 %	- 30 %	25 %
23.11.16	4 %	29 %	- 20 %	13 %
11.12.16	75 %	13 %	2 %	31 %
12.12.16	93 %	26 %	-18 %	11 %
13.12.16	33 %	38 %	58 %	10 %
18.12.16	5 %	13 %	8 %	12 %
03.01.17	51 %	28 %	-12 %	44 %
24.01.17	76 %	11 %	- 29 %	8 %
25.01.17	58 %	24 %	- 31 %	23 %

830

831

832

833

Atmospheric
Chemistry
and Physics
Discussions

834   Table 3: Summary of secondary aerosol components, both organics and inorganics. The mass
835   concentration is represented as mean ± standard deviation (µg m^{-3}) for the five clusters.

Cluster	Sulfate	Nitrate	Ammonium	HOA	BBOA	OOA
C1	3.5 ± 3.1	1.0 ± 1.0	1.5 ± 1.2	0.9 ± 1.3	2.1 ± 2.4	4.0 ± 2.7
C2	2.9 ± 1.7	0.9 ± 1.0	1.0 ± 0.8	0.7 ± 1.3	1.6 ± 2.2	3.1 ± 2.1
C3	3.4 ± 3.0	1.1 ± 0.9	1.5 ± 1.2	0.8 ± 1.1	1.5 ± 2.2	3.5 ± 2.6
C4	1.2 ± 0.9	0.5 ± 0.4	0.6 ± 0.4	0.8 ± 1.8	1.3 ± 1.8	1.7 ± 1.1
C5	1.4 ± 1.7	1.0 ± 1.1	1.1 ± 0.8	0.6 ± 0.9	1.3 ± 1.3	2.0 ± 1.4

836

837

838

839

840

841